

Estimation of HRV and SpO2 from Wrist-Worn Commercial Sensors for Clinical Settings

Delaram Jarchi*, Dario Salvi, Carmelo Velardo, Adam Mahdi, Lionel Tarassenko and David. A. Clifton

Abstract— We describe an evaluation of photoplethysmography (PPG) signals with two wavelengths channels (infrared and red) using a wrist-worn sensor for the estimation of heart rate variability (HRV) and oxygen saturation (SpO2). Five healthy subjects were equipped with a commercial wrist-worn pulse oximeter (Wavelet Health, USA) on the right hand, and both a commercial smart watch for fitness use (Huawei Watch, Series 2) and a clinically-validated transmission-mode pulse oximeter (Creative Medical PC-68B) on their left hand as a reference. Synchronised PPG signals from the Wavelet Health, the Huawei watch, and the PC-68B were recorded for approximately 10 minutes. Subjects were asked to leave the left hand in a resting and steady state, while moving the right hand with two types of movement (periodic and random). A method is proposed here to incorporate coupling information between the two wavelengths of PPGs based on the bivariate empirical mode decomposition algorithm. Our method is shown to improve the quality of red PPG allowing improved estimation of SpO2. A comparison of average heart rate (HR), HRV, and SpO2 from the three devices is provided, as a big step towards reliable estimation of HRV and SpO2 from wrist-worn sensors.

I. INTRODUCTION

PPG-based monitoring is often used in vital-sign monitoring for the estimation of heart rate, blood-oxygen saturation, and respiratory rate. The ability of PPG-acquisition to be integrated into wearable devices provides the potential for unobtrusive tracking of vital signs [1] suitable for continuous monitoring of patient's conditions including acute patients in the hospital and the management of chronic disease in home environment.

Clinically-validated pulse-oximeters are typically based on transmission-mode PPG, which requires the user to wear a probe on a finger [2] or an earlobe [3]. Recently wearables sensors and smart watches have started using reflectance-mode PPG to gather vital signs, usually for fitness purposes. However, these devices have not been widely used in everyday clinical practice. The main challenge in the use of reflectance pulse oximeters is their sensitivity to motion as they can be easily contaminated with motion artefacts due to poor sensor detachment anytime there is an air gap between the sensor and skin. These could result in poor estimation of vital signs.

There are numerous techniques to estimate average heart rate or heart rate variability [4] from reflectance PPG. The estimation of oxygen saturation (SpO2) requires two LEDs with two different wavelengths to be recorded. Although there are a number of commercial devices which enable

estimation of SpO2 from transmission PPG, the estimation from reflectance devices is poorly studied. Attempts in detecting SpO2 from reflectance PPG focus on wrist worn sensors [5] and video recordings [6].

This paper focuses on improving the quality of reflectance PPG signals to enable robust estimation of SpO2. The proposed method jointly decomposes the two-wavelengths of PPG signals (red and infrared) into the desired heart rate frequency rhythm to increase the quality of the red signal which has shown to be of lesser quality than the infrared signal. We used the Wavelet Health sensor to collect two wavelengths of PPG for the estimation of average HR, HRV and SpO2. A reference for the PPG waveform was captured using a Huawei Series 2 smart watch programmed with an Android Wear mobile application to get raw PPG waveforms from only one LED to estimate HR and HRV. The device was chosen because it uses a green LED, which is known to produce better heart rate estimations than via red light [7], and which yields good-quality signals at rest. The PC-68B pulse oximeter device has been used as a reference for the SpO2 estimates.

The remainder of the paper is as follows. In Section II, details of the experiments are provided. In Section III, the proposed technique to effectively filter the AC component of the red PPG signal is provided. Our results are discussed in Section IV. Section V concludes the paper by highlighting advantages of using the method and describing potential improvements for future studies.

II. EXPERIMENTS

Five healthy subjects volunteered to take part in our experiments. During 10 minutes, synchronised signals were recorded using the Wavelet Health wristband, a Huawei watch Series 2, and a PC-68B pulse oximeter. A subject wearing the sensors is shown in Fig. 1. For all subjects, the left hand wearing the Huawei watch and the PC-68B remained at rest and was used to generate reference signals. Subjects were asked to wear the Wavelet Health sensor on the right hand and move it periodically up and down for one minute starting at third minute. Then, subjects were asked to move their hand in random directions for one minute starting at sixth minutes.

To estimate SpO2, the DC and AC components of the red and infrared signals need to be accurately separated from raw PPG waveforms. In the case of the Wavelet Health sensor, the red signal has lower quality than infrared signal. The proposed technique integrates the AC components of the red and infrared signals as a complex waveform and then

This work was supported by EPSRC grant.

*D. Jarchi is with Engineering Science Department, University of Oxford, OX3 7DQ. delaram.jarchi@eng.ox.ac.uk



Fig. 1. A subject wearing the Wavelet Health wristband on the right wrist; and the Huawei watch series 2 and a PC-68B pulse oximeter on the left hand.

bivariate empirical mode decomposition (EMD) algorithm [8] as a complex EMD algorithm has been applied. This helps to recover the main oscillation of the red signal in places the actual pulse has been lost due to noises and other interferences.

After applying the complex EMD algorithm, the Hilbert transform has been used to obtain a reference signal from both imaginary and real part of the signals given by the complex EMD algorithm. The reference signal has been used as an input to the normalised least mean squares (NLMS) algorithm to filter the AC component of the red signal. In the following, the basic algorithms, including explanation of their usage in the proposed platform, have been briefly described. In the last part of this section, the formulations used for the estimation of SpO2 are provided.

A. Bivariate Empirical Mode Decomposition

The standard empirical mode decomposition algorithm [9] was developed to adaptively decompose a real signal into a finite set of components called intrinsic mode functions (IMFs). Several extensions of the EMD algorithm have been proposed to operate on the complex data. One popular method is the bivariate EMD algorithm [8], which is summarised in the following steps.

Step 1: Determine the number of projections (N) and directions as $\varphi_k = \frac{2k\pi}{N}$, $k \in [1, N]$. Then complete the steps 2-4.

Step 2: Project the complex value signal $x(t)$ in directions φ_k as $p_{\varphi_k}(t) = \text{Re}\{e^{-j\varphi_k}x(t)\}$.

Step 3: Find all local maxima of φ_k and their corresponding locations as $\{t_j^k, x(t_j^k)\}$.

Step 4: Interpolate the set $\{t_j^k, x(t_j^k)\}$ (using spline interpolation) to obtain an envelope curve in direction φ_k as $e_{\varphi_k}(t)$.

Step 5: Calculate the mean $m(t)$ of all envelope curves via $m(t) = \frac{1}{N} \sum_k e_{\varphi_k}(t)$.

Step 6: Subtract the mean from the input signal $x(t)$ to extract an oscillatory component $d(t) = x(t) - m(t)$.

Then, $d(t)$ needs to be examined whether it satisfies the requirements of an IMF. If not, $d(t)$ must be regarded as

original signal and steps 1-6 should be repeated until an IMF is found and is recorded. Then, the residual component will be formed by subtracting the resulted IMF from the original signal where it is subjected to previous iterations until all IMFs are found.

B. Singular Spectrum Analysis

Singular Spectrum Analysis (SSA) as a model-free technique has been extensively applied to time-series data to decompose it into a number of orthogonal components including slowly-varying trends, oscillations, and unstructured noise. SSA has been successfully used in many times-series analysis applications including denoising and prediction [10]. It has shown to be suitable for the separation of noise from oscillatory components of the acceleration signals for gait analysis. The SSA algorithm contains two main steps: decomposition and reconstruction.

Step 1: Decomposition: This step consists of two stages called embedding and singular value decomposition (SVD). In the embedding stage, a multidimensional matrix called the trajectory matrix is created from a delayed version of the input time-series. Based on this, the time-series s of length n is converted into an $l \times k$ matrix as the trajectory matrix:

$$\mathbf{X} = [x_{ij}] = [\mathbf{x}_1, \mathbf{x}_2, \dots, \mathbf{x}_k] = \begin{bmatrix} s_0 & s_1 & s_2 & \dots & s_{k-1} \\ s_1 & s_2 & s_3 & \dots & s_k \\ s_2 & s_3 & s_4 & \dots & s_{k+1} \\ \vdots & \vdots & \vdots & \ddots & \vdots \\ s_{l-1} & s_l & s_{l+1} & \dots & s_{n-1} \end{bmatrix} \quad (1)$$

where $k = n - l + 1$ and l is the window length (embedding dimension) ($1 \leq l \leq n$). In the next stage, SVD is applied to the trajectory matrix for decomposition and representation as a sum of rank-one bi-orthogonal elementary matrices.

Therefore, the eigenvalues ($\lambda_1, \lambda_2, \dots, \lambda_l$) and the corresponding eigenvectors ($\mathbf{u}_1, \mathbf{u}_2, \dots, \mathbf{u}_l$) of $\mathbf{S} = \mathbf{X}\mathbf{X}^T$ can be obtained assuming that they are sorted in decreasing order of magnitudes ($\lambda_1 \geq \lambda_2 \geq \dots \geq \lambda_l \geq 0$).

If $\mathbf{v}_i = \mathbf{X}^T \mathbf{u}_i / \sqrt{\lambda_i}$, then it is possible to express the trajectory matrix as:

$$\mathbf{X} = \mathbf{X}_1 + \mathbf{X}_2 + \dots + \mathbf{X}_d \quad (2)$$

where $d = \arg\max_i \{\lambda_i > 0\}$ and $\mathbf{X}_i = \sqrt{\lambda_i} \mathbf{u}_i \mathbf{v}_i^T$. The vector \mathbf{u}_i is the i th left eigenvector, the vector \mathbf{v}_i is the i th right eigenvector, and the collection $(\sqrt{\lambda_i}, \mathbf{u}_i, \mathbf{v}_i)$ is called the i th eigentriple of the SVD in Equation (2).

Step 2: Reconstruction: In this step, m disjoint subsets are formed using eigentriples. By setting the indices for subsets (I_1, I_2, \dots, I_m), the elementary matrices of each group can be summed together to form:

$$\mathbf{X}_{I_j} = \mathbf{X}_{i_{j1}} + \dots + \mathbf{X}_{i_{jp}} \quad (3)$$

where $I_j = i_{j1}, \dots, i_{jp}$. The original trajectory matrix can be expressed as the sum of all the resulted matrices \mathbf{X}_{I_j} :

$$\mathbf{X} = \mathbf{X}_{I_1} + \dots + \mathbf{X}_{I_m} \quad (4)$$

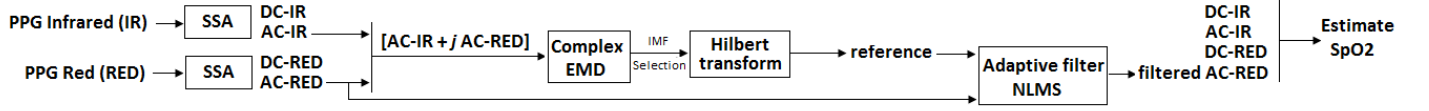


Fig. 2. Diagram of the proposed algorithm which aims to improve the quality of the red PPG signal. The DC-removed components of both red and infrared signals using the Singular Spectrum Analysis (SSA) algorithm have been combined as a complex input to the bivariate empirical mode decomposition algorithm.

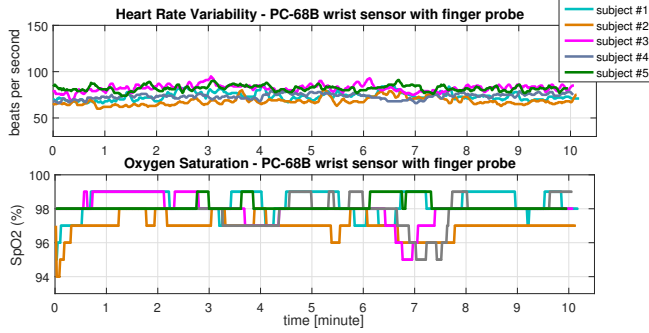


Fig. 3. *Upper plot*: Estimated heart rate per second from the finger probe using PC-68B pulse oximeter for five subjects. *Lower plot*: Estimated SpO2 values using PC-68B.

Grouping of the eigentriples is an application-specific task and therefore there are no fixed rules for this purpose. The final step of the SSA algorithm is diagonal averaging in which the final elementary matrix, which is the sum of all elementary matrices in the group, is transformed into a time-series of length n . In our work, SSA has been used to separate the DC and AC components of the red and infrared signals. The resulting eigenvector with largest eigenvalue ($I_1 = 1$) has been used to extract the DC component and the eigenvectors related to the second- and third-largest eigenvalues ($I_2 = 2, 3$) are grouped to form a denoised version of the AC component.

C. Hilbert transform

The Hilbert transform (HT) [9] is typically applied to narrow-band signals to give an instantaneous time-frequency distribution. It has been previously applied to IMFs derived from the EMD algorithm. The discrete HT can be used to compute the analytic signal of the input narrow-band signal. The discrete HT denoted by $\mathbf{H}_d[\cdot]$ of signal $x(t)$ is given by:

$$\mathbf{H}_d[x(t)] = \sum_{\substack{\delta=-\infty \\ \delta \neq t}}^{+\infty} \frac{x(\delta)}{t - \delta} \quad (5)$$

The analytic version of the input $d(t)$ signal is defined as:

$$C(t) = d(t) + J\mathbf{H}_d[d(t)] = a(t)e^{j\theta(t)} \quad (6)$$

$$d(t) = \Re(a(t)e^{j\theta(t)}) = a(t)\cos(\theta(t)) \quad (7)$$

where $J = \sqrt{-1}$ and $a(t)$ and $\theta(t)$ are the instantaneous amplitude and phase of the input respectively. The advantage of using the analytic signal is to obtain instantaneous quantities such as phase, energy, and frequency.

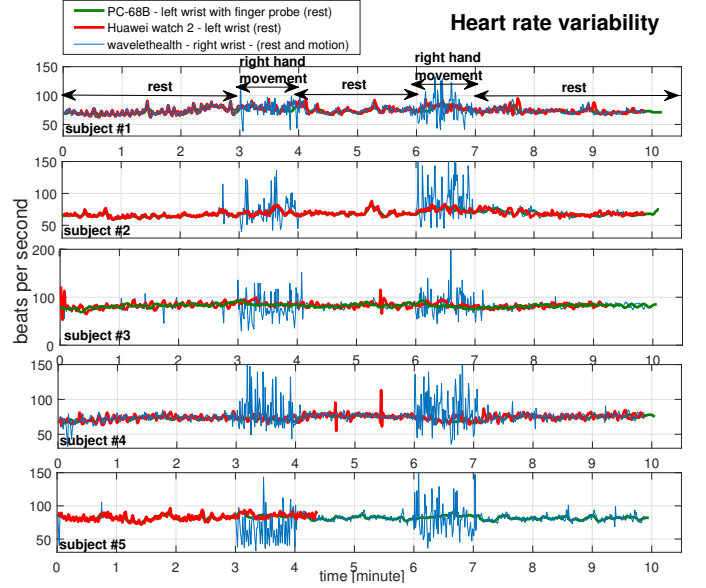


Fig. 4. instantaneous heart rate estimated from Huawei watch and PC-68B in the rest state versus estimation from the Wavelet Health sensor during the rest and motion. There is a good agreement in the rest period between instantaneous heart rate estimates to indicate HRV.

In our work, the instantaneous amplitude and phase of the imaginary and real parts of the complex EMD output are combined to create a reference signal for AC components. Denoting the input signal to the complex EMD algorithm as $p_{IR}(t) + jp_R(t)$, where $p_{IR}(t)$ is the AC component of the infrared signal and $p_R(t)$ is the AC component of the red signal, both after DC removal using the SSA algorithm. The reference signal can be constructed using:

$$\begin{aligned} \phi(t) &= [2\cos(\theta_R(t)/2)\cos(\theta_{IR}(t)/2) - 1], \\ r(t) &= \sqrt[2]{a_{IR}(t)a_R(t)}\phi(t) \end{aligned} \quad (8)$$

where $\theta_{IR}(t)$ and $\theta_R(t)$ are the instantaneous phase of the real and imaginary parts of the sum of selected IMFs after applying the complex EMD algorithm. $a_{IR}(t)$ and $a_R(t)$ are the corresponding instantaneous amplitudes. The reference $r(t)$ is used in the next section by the NLMS algorithm to retrieve the main oscillation of the AC component of the red PPG signal.

D. Normalised least mean squares filter

The NLMS adaptive filters are a variation of LMS filters that use a normalisation of the power of the input signal. Consider the error between measured AC component of the

red PPG signal $p_R(t)$ and desired signal is obtained using the following equation:

$$e(t) = r(t) - \mathbf{h}^T(t)\mathbf{p}_R(t) \quad (9)$$

where $r(t)$ is the reference signal created using the output of the complex EMD algorithm and the Hilbert transform, $\mathbf{p}_R(t)$ is a vector of length L (filter order) from the AC component of the red PPG signal following applying the SSA algorithm as the input of the adaptive filter, and $\mathbf{h}^T(t)$ is the filter coefficient (weight) vector. The NLMS filter uses steepest descent, to find filter weights that minimises the mean square error. Therefore, the linear update equation is obtained as:

$$\mathbf{h}(t+1) = \mathbf{h}(t) + \frac{\mu}{\|\mathbf{p}_R(t)\|^2} \mathbf{p}_R(t)e(t) \quad (10)$$

μ is the step size. The output of the filter as $y(t) = \mathbf{h}^T(t)\mathbf{p}_R(t)$ has been used as the filtered AC component of the red PPG signal AC_R .

E. Estimation of SpO2

SpO2 values can be calculated using the following formula:

$$SpO2 = 110 - 25R \quad (11)$$

where R is the ratio of red and infrared signals:

$$R = \frac{AC_R/DC_R}{AC_{IR}/DC_{IR}} \quad (12)$$

and where AC_R and DC_R denote the AC and DC components of the red PPG signal, and AC_{IR} and DC_{IR} denote the AC and DC components of the infrared PPG signal. For this ratio, AC_R has been calculated based on the difference between the maximum and minimum of the AC component. The DC component has been evaluated at a point between corresponding points related to the maximum and minimum of the AC component. The SSA method has been used to decompose the red and infrared signals into AC and DC components. The AC component of the red PPG signal has been filtered using the proposed algorithm as explained earlier in this section.

III. RESULTS

The estimated heart rate and SpO2 every second given by the PC-68B for five subjects are shown in Fig. 3. As it can be seen from this figure, subject #2 had the lowest heart rate and SpO2 for most of the duration of the experiments. The instantaneous heart rate estimated from the PPG signal of the Huawei watch for all the subjects are plotted in Fig. 4 (shown in red), which are overlapped well with the HR estimates every second from the PC-68B system (shown in green), showing good agreement between the two. In this figure, also the HRV estimation using the Wavelet Health sensor based on detecting peaks in the infrared signal has also been plotted (shown in blue).

As can be seen in Fig. 4, in segments where the right hand is moving, the HRV estimations deviate from normal

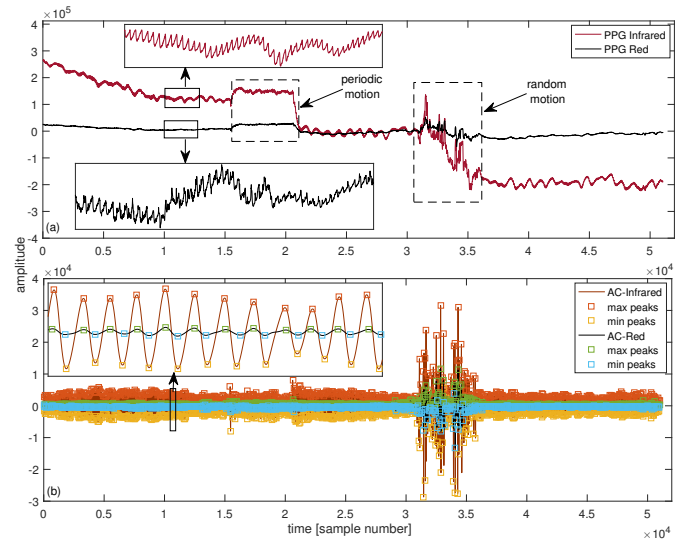


Fig. 5. Upper plot: Mean removed raw infrared and red signals. Lower plot: The peaks are located in the extracted AC component of red and infrared.

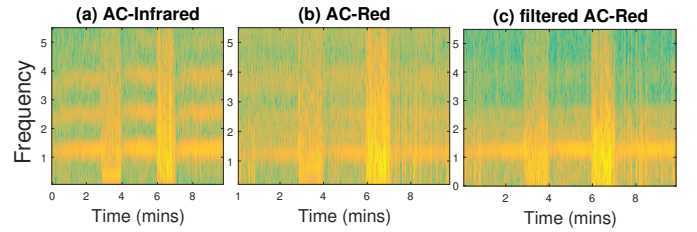


Fig. 6. STFT of the AC component of the infrared signal (a) and red signal (b). (c) The STFT of the filtered AC component of red signal for subject #4 using the proposed algorithm.

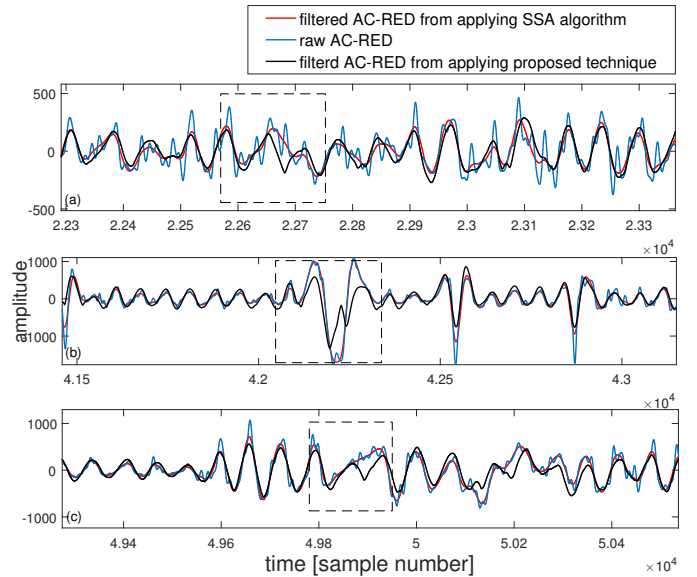


Fig. 7. (a-c) Segments of the data which present the effectiveness of applying the proposed technique to restore dissolved red PPG signal cycles.

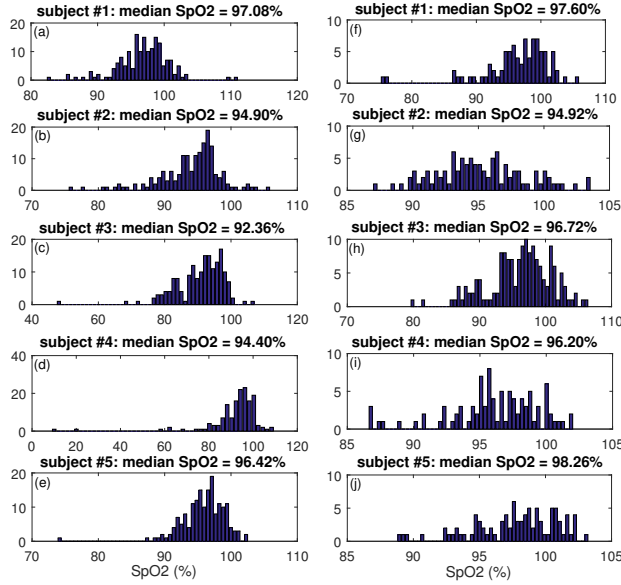


Fig. 8. (a-e) Histogram of the estimated SpO2 values for two minutes starting at first minute of the experiment. (f-j) Histogram of the estimated SpO2 values during one minute in the last part of the experiment.

heart rate estimates. For subject #5 half of the signals from the Huawei watch were lost. In Tables I and II, a selected HRV measure of RMSSD (the square root of the mean of the squares of the successive differences between adjacent RRs) in milliseconds is compared between the estimates from the Huawei watch and the Wavelet Health sensor for data from minute #1 to #2 and minute #8 to #9 respectively. The average heart rate for these segments in terms of beats per minute is compared among all three devices, which shows very good agreement.

The most challenging part of our work has been the estimation of SpO2 using the Wavelet Health wrist-worn device. As explained in previous sections, the AC and DC components of the red and infrared signals need to be accurately separated and filtered. In Fig. 5, for a selected subject, the raw infrared and red signals and the estimated AC and DC components, including detected peaks, are shown. In Fig. 6(a,b), the spectrogram of the AC component of the infrared and red signal from subject #4 has been shown. This figure shows that the spectrum of the AC-Infrared is of highest quality. The STFT of the filtered AC component of the red signal is shown in Fig. 6(c). In Fig. 7, three selected segments of signals for the subject #4 are shown, where the AC component of the cycle frequency of the red signal has been recovered using the proposed algorithm.

Using the PC68-B system, SpO2 has been averaged in a two-minute window (minute #1 to #3) and one minute window (minute #8.5 to #9.5) for five subjects and calculated as (98.6%, 97.4%, 98.8%, 98.0% and 98.1%) and (98.4%, 97.0%, 98.0%, 98.0% and 98.0%), respectively.

The histogram of SpO2 estimations using the Wavelet Health sensor is provided in Fig. 8 (a-e) and Fig. 8 (f-j) for the selected 2-minute window at the beginning of the

TABLE I
COMPARISON OF HRV FOR MINUTE #1 TO #2

subject ID	RMSSD(ms)		mean HR (BPM)		
	Huawei	Wavelet Health	Huawei	Wavelet Health	PC-68B
#1	50.45	55.79	71.59	71.56	70.54
#2	30.78	39.52	64.04	64.08	63.21
#3	26.98	58.17	81.88	81.95	82.22
#4	30.22	45.03	74.44	74.21	73.5
#5	30.77	42.81	80.84	80.86	80.63

TABLE II
COMPARISON OF HRV FOR MINUTE #8 TO #9

subject ID	RMSSD(ms)		mean HR (BPM)		
	Huawei	wavelet health	Huawei	wavelet health	PC-68B
#1	24.74	40.65	72.95	72.79	73.37
#2	29.80	35.42	66.75	67.02	66.65
#3	26.14	36.94	78.32	79.50	83.08
#4	32.41	71.11	74.92	75.11	74.29
#5	NA	41.64	NA	81.45	81.06

experiment and a 1-minute window in the last part of the experiments. The median of the estimations are shown in this figure. For subject #2, the estimated median SpO2 for both time-windows presents a lower value when compared to subject #1 and #5. This is in-line with estimated SpO2 using the PC68-B (see Fig. 3). There is good estimation for subjects #1 and #5.

IV. DISCUSSION

In this paper a method has been proposed to improve the estimation of AC components of two-wavelength PPGs. This will be a basis for future studies to exploit mutual coupling information of two-wavelength PPGs to further improve the resulting SpO2 estimates. Although errors of approximately 3% may exist for the estimation of SpO2 from commercial devices such as the PC-68B system, the SpO2 results obtained for most subjects via the Wavelet Health device seem reasonable. For extensive evaluation of the Wavelet Health sensor, various SpO2 levels (potentially requiring deoxygenation of the subject) need to be generated and compared. The equation for estimation of SpO2 which uses the ratio of the AC and DC components can be further calibrated to obtain more reliable SpO2 values. Furthermore, estimation of HRV where there are hand movements or motion artefact should be studied from joint time-frequency representations of the PPG signals.

The results for heart rate variability and average heart rate have been in good agreement between the Wavelet Health sensor, the Huawei watch Series 2, and the PB-68B. Overall, the Wavelet Health sensor as a wrist-worn device has been shown to produce high-quality signals which are useful for the estimation of heart rate variability and SpO2; and which could also be used for estimating respiratory rate, in future studies including various patient cohorts.

ACKNOWLEDGMENT

The authors would like to thank Wavelet Health company for offering an evaluation kit to record raw PPG signals from their developed wrist worn sensor. They also thank the

Google Wear team and Huawei for giving help to access the raw signals of the smart watch.

REFERENCES

- [1] L. Tarassenko, D. A. Clifton, M. R. Pinsky, M. T. Hravnak, J. R. Woods, P. J. Watkinson Centile-based early warning scores derived from statistical distributions of vital signs in Resuscitation, vol. 82, no. 8, 2011, pp. 1013-1018.
- [2] S. Bagha, L. Shaw, A Real Time Analysis of PPG Signal for Measurement of SpO₂ and Pulse Rate in International Journal of Computer Applications, vol. 36, no. 11, 2011.
- [3] K. Budidha, P. A. Kyriacou, "Development of an optical probe to investigate the suitability of measuring photoplethysmographs and blood oxygen saturation from the human auditory canal" in Conf Proc IEEE Eng Med Biol Soc., 2013, pp. 1736-1739.
- [4] D. Jarchi, A. J. Casson, "Towards Photoplethysmography-Based Estimation of Instantaneous Heart Rate During Physical Activity" in IEEE Transactions on Biomedical Engineering, vol. 64, no. 9, 2017, pp. 2042-2053.
- [5] A. M. Tuan, A. Young, E. Wentink, F. Wieringa, "Characterization and reduction of motion artifacts in photoplethysmographic signals from a wrist-worn device" in Conf Proc IEEE Eng Med Biol Soc., 2015, pp. 6146-6149.
- [6] L. Tarassenko, M. Villarroel, A. Guazzi, J. Jorge, D. A. Clifton, C. Pugh, "Non-contact video-based vital sign monitoring using ambient light and auto-regressive models" in Physiological measurement, vol. 35, no. 5, 2014, pp. 807-831.
- [7] J. Lee, K. Matsumura, K. I. Yamakoshi, P. Rolfe, S. Tanaka, T. Yamakoshi "Comparison between red, green and blue light reflection photoplethysmography for heart rate monitoring during motion" in Engineering in Medicine and Biology Society (EMBC), 2013 35th Annual International Conference of the IEEE (pp. 1724-1727). July 2013.
- [8] G. Rilling, P. Flandrin, P. Goncalves, J. M. Lilly, "Bivariate Empirical Mode Decomposition" in IEEE Signal Processing Letters, vol. 14, no. 12, 2007.
- [9] N. E. Huang, Z. Shen, S. R. Long, M. C. Wu, H. H. Shih, Q. Zheng, N. C. Yen, C. C. Tung, H. H. Liu, "The empirical mode decomposition and Hilbert spectrum for nonlinear and non-stationary time series analysis" in Proc Roy Soc London A, vol. 454, 1998, pp. 903-995.
- [10] D. Jarchi, C. Wong, R. M. Kwasnicki, B. Heller, G. Tew, G.-Z. Yang, "Gait Parameter Estimation from a Miniaturised Ear-Worn Sensor using Singular Spectrum Analysis and Longest Common Subsequence" in IEEE Transactions on Biomedical Engineering, vol. 61, no. 4, 2014, pp. 1261-1273.